Observation of ionospherically reflected quasiperiodic emissions by the DEMETER spacecraft

Miroslav Hanzelka, Ondřej Santolík, Mychajlo Hajoš, František Němec, Michel Parrot

AGU PUBLICATIONS

Geophysical Research Letters

RESEARCH LETTER
10.1002/2017GL074883

Key Points:
- Quasiperiodic emissions observed on low-Earth orbit show an unexpected change of their wave vector direction
- This peculiar pattern is explained by ionospheric reflection of the downward propagating waves
- These emissions are probably guided down to the Earth by the plasmapause density gradient

Correspondence to:
M. Hanzelka,
mirekhanzelka@gmail.com

Citation:
Hanzelka, M., O. Santolik, M. Hajoš, F. Nemec, and M. Parrot (2017), Observation of ionospherically reflected quasiperiodic emissions by the DEMETER spacecraft, *Geophys. Res. Lett.*, *44*, 8721–8729, doi:10.1002/2017GL074883.

Received 11 JUL 2017
Accepted 12 AUG 2017
Accepted article online 16 AUG 2017
Published online 9 SEP 2017

Observation of ionospherically reflected quasiperiodic emissions by the DEMETER spacecraft

Miroslav Hanzelka[1,2], Ondřej Santolík[1,2], Mychajlo Hajoš[2], František Němec[1], and Michel Parrot[3]

[1]Faculty of Mathematics and Physics, Charles University, Prague, Czech Republic, [2]Department of Space Physics, Institute of Atmospheric Physics, The Czech Academy of Sciences, Prague, Czech Republic, [3]LPC2E/CNRS, Orléans, France

Abstract Quasiperiodic (QP) electromagnetic emissions are whistler mode waves at typical frequencies of a few kHz characterized by a periodic time modulation of their intensity. The DEMETER spacecraft observed events where the QP emissions exhibit a sudden change in the wave vector and Poynting vector directions. The change happens in a short interval of latitudes. We explain this behavior by ionospheric reflection and present a ray-tracing simulation which matches resulting wave vector directions. We also attempt to locate the source region of these emissions and conclude that they are most probably generated at the inner boundary of the plasmapause which also acts as a guide during the propagation of the QP emissions.

1. Introduction

Quasiperiodic (QP) electromagnetic emissions are whistler mode waves characterized by a periodic intensity modulation with the period ranging from about 10 s up to several minutes [see e.g., *Helliwell*, 1965; *Sazhin and Hayakawa*, 1994; *Smith et al.*, 1998]. During the last decades there were numerous observations of QP emissions by both ground stations and satellites. Historically, we divide QP emissions into two types, QP1 and QP2 [*Sato et al.*, 1974]. The first type (QP1) is associated with ultralow frequency (ULF, 1 mHz–1 Hz) pulsations of Earth's magnetic field. *Kimura* [1974] proposed that this type of emissions originates due to quasiperiodic modulation of resonance condition for wave growth in the source region. The second type (QP2 emissions) is observed when ULF magnetic field pulsations are absent and their generation mechanism is still unclear. *Davidson* [1979] proposed a mechanism based on the relaxation oscillations of the cyclotron instability. Another suggested explanation assumes that the QP2 emissions result from an auto-oscillation regime of wave generation [*Bespalov*, 1981; *Pasmanik et al.*, 2004]. Conjugate observations of precipitating high-energy electrons and QP2 emissions by the DEMETER (Detection of Electro-Magnetic Emissions Transmitted from Earthquake Regions) spacecraft indicated a connection between QP2 events and precipitation of high-energy electrons [*Hayosh et al.*, 2013]. Nonetheless, the strict division of QP1 and QP2 based on the generation mechanism becomes less certain when various spacecraft data are taken into account [*Tixier and Cornilleau-Wehrlin*, 1986].

For many years the main source of data on QP emissions was measurements from ground stations. Examples of larger statistics obtained from ground-based data were shown, e.g., by *Smith et al.* [1998]. With the advent of multicomponent measurements on low-orbit satellites, studies of propagation properties of QP emissions became possible, removing thus the selection effect of waves which are able to penetrate the ionosphere to the ground stations. For example, distinct characteristics of wave propagation at the low-Earth orbit at high latitudes from 55° to 65° were analyzed by *Santolík and Parrot* [1999] and *Pasmanik et al.* [2004] using data from the Freja spacecraft, and by theoretical modeling of *Bortnik et al.* [2011].

Using the data from the DEMETER spacecraft, *Hayosh et al.* [2016] recently analyzed wave properties of QP emissions, mainly the direction of the Poynting vector and the direction of the wave vector, as a function of the geomagnetic latitude. They show that values of the polar angle θ_{kB} between the wave vector direction and the local magnetic field $\mathbf{B_0}$ are always well below 90° at high latitudes in the Northern Hemisphere and well above 90° in the Southern Hemisphere, indicating propagation from the magnetosphere toward the Earth in both cases. In the present paper we focus on events where the properties of QP emissions observed

by DEMETER at an altitude of 660 km deviate from these statistical results, exhibiting a sudden change of propagation parameters which suggests that an apparent source of a part of the emission is located close to the Earth, below the spacecraft altitude.

We propose a propagation scheme where the emission exhibiting unusual features results from an ionospheric reflection of the original direct QP emission propagating toward the Earth's surface. In section 2 we describe properties of QP emissions in those unique events. In section 3 we conduct a ray-tracing simulation based on measured wave parameters and compare it with a sample event, and in section 4 we attempt to locate the source of the observed emissions with the use of backward ray tracing. Finally, in section 5 we discuss the validity of our model and summarize our results.

2. Data

The data were collected by the French microsatellite DEMETER. This spacecraft was launched in June 2004, and its mission ended in December 2010. DEMETER was placed on a nearly Sun-synchronous orbit (at local time sectors around 10 h and around 22 h) at an altitude of about 660 km, collecting data in a range of geomagnetic latitude λ_{mag} from −65° to 65°. During its 6 year mission the satellite collected 196 QP events in the burst mode [*Hayosh et al.*, 2016], providing multicomponent data sampled at 2500 Hz for a detailed analysis of wave propagation using the methods outlined by *Santolík et al.* [2006]. However, as the burst mode was mostly triggered at lower latitudes, data from latitudes higher than 50° were available only in about 140 cases of QP events. According to the results of *Hayosh et al.* [2016], the observed direction of the Poynting vector is mostly downward, nearly perpendicular to the ground, and the dependence of θ_{kB} on λ_{mag} is fairly linear, decreasing from $\theta_{kB} \approx 70°$ at $\lambda_{mag} = 50°$ to $\theta_{kB} \approx 30°$ at $\lambda_{mag} = 60°$.

Altogether, 26 events in this data set exhibit a sudden and surprising change of θ_{kB} as a function of geomagnetic latitude λ_{mag}, where the θ_{kB} values jump from 30° to 70° at higher latitudes to the interval of about 130°–170° at lower latitudes. Figure 1 shows an example case of 13 April 2006, 19:25:00–19:27:00 UT. In Figures 1a and 1b we, respectively, plot frequency-time spectrograms of magnetic field and electric field power spectral density, where we clearly see QP emissions at frequencies between 700 and 1200 Hz, exhibiting a modulation of wave intensity with a period of 20 s. Largest electric field and magnetic field intensities are observed between 800 Hz and 1100 Hz. For further analysis we applied a threshold of 10^{-5} $mV^2m^{-2}Hz^{-1}$ for the electric field to remove the background noise from our results. For each time-frequency interval above this threshold we computed spectral matrices from the six-dimensional measurements of electric and magnetic fields using the 1024-point fast Fourier transform with Hanning windows and 50% overlap and averaged them over three neighboring time domain windows. The resulting time resolution is $\sim$ 620 ms, with a frequency resolution of $\sim$ 2.5 Hz up to the Nyquist frequency of 1.25 kHz. These matrices were used as the input for calculation of wave propagation parameters, namely the angle θ_{kB} between the wave vector and the ambient magnetic field, the azimuth ϕ_{kB} of the wave vector with respect to the plane of the local magnetic meridian, planarity, and ellipticity—Figures 1c–1f, respectively. The calculations were done according to the singular value decomposition (SVD) methods described by *Santolík and Gurnett* [2002] and *Santolík et al.* [2003]. The polar angle θ_{kB} is defined on the interval (0°, 180°) since we use an electromagnetic SVD method which takes into account both electric and magnetic field measurements. The transition from earthward to anti-earthward propagation is clearly observed at λ_{mag} between 55° and 53°, corresponding to McIlwain's parameter L between 3.4 and 3.1 where θ_{kB} changes from 50°–80° to 120°–150° (Figure 1c). The azimuthal angle ϕ_{kB} is obtained in the interval (−180°, 180°) where $\phi_{kB} = 0°$ means outward in the sense of increasing L shells. The obtained values consistently show the opposite (inward) direction (Figure 1d). Ellipticity of the magnetic field polarization (Figure 1e) shows right-handed polarization which corresponds to QP emissions propagating in the whistler mode. High values of the magnetic field planarity (Figure 1f) are consistent with our wave normal calculations in the time-frequency intervals where we initially observe downward propagation and subsequently the upward propagation with a transition zone of low planarity between them. In this zone, a mixture of waves propagating in different directions is expected. The Poynting vector direction (Figure 1g), calculated with the spectral method of *Santolík et al.* [2010] also shows this transition from 0° to 180°.

All the other identified cases of QP emissions with anomalous θ_{kB} dependence on (λ_{mag}) were also observed at high geomagnetic latitudes from 50° to 60°, which correspond to the range from $L = 2.5$ to $L = 4.0$ approximately. The periods of these QP emissions were shorter than or comparable to 20 s.

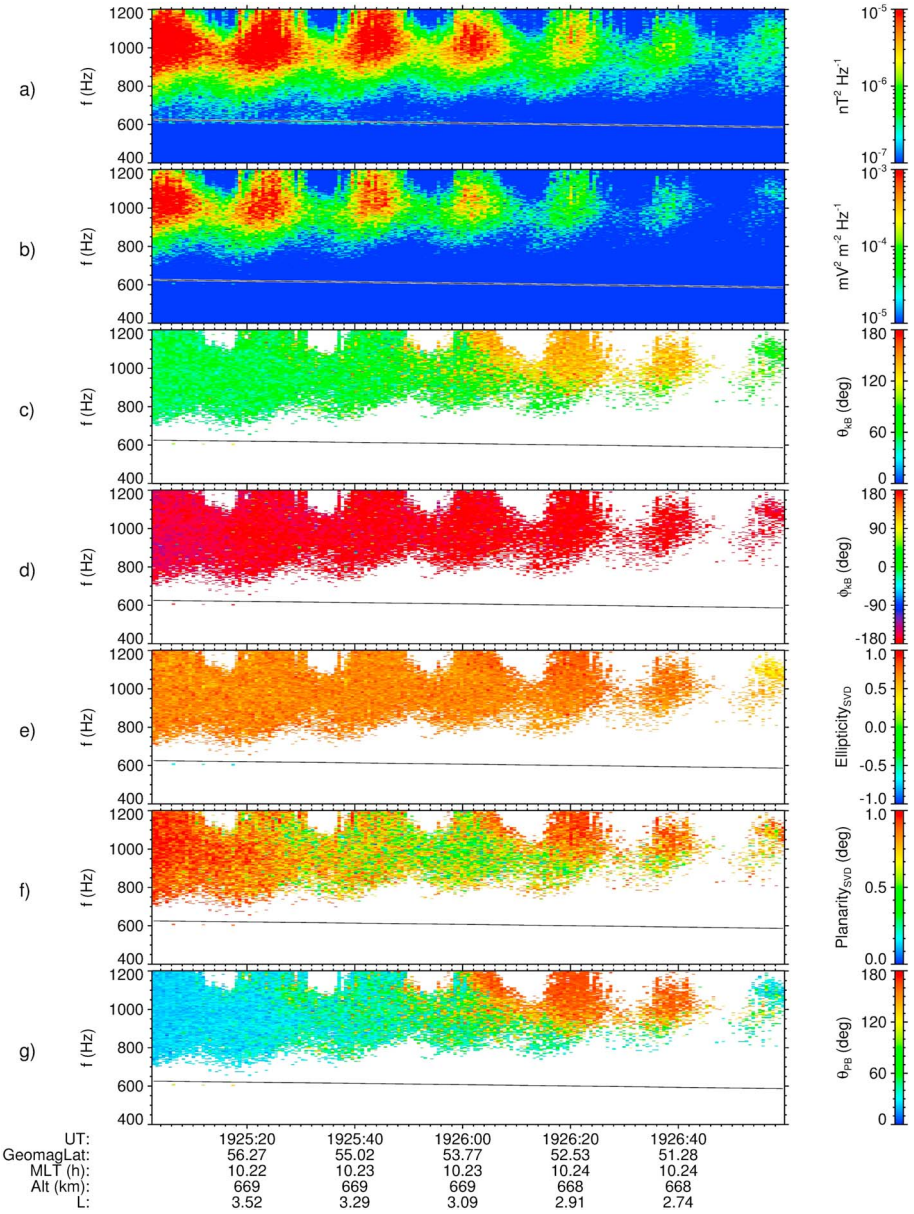

Figure 1. Frequency-time spectrograms of a QP event observed on 13 April 2006. (a) Magnetic field power spectral density, (b) electric field power spectral density, (c) polar angle θ_{kB}, (d) azimuthal angle ϕ_{kB}, (e) ellipticity, (f) planarity, and (g) polar angle θ_{PB} of the Poynting vector. The solid line shows the local proton gyrofrequency.

3. Interpretation

The hypothesis we propose to explain our observations is based on ionospheric reflection of the originally earthward propagating waves. We assume that the waves are propagating downward, to the geomagnetic latitudes between 53° and 57°. Then, according to the Snell's law, they are reflected at the bottom side base of the ionospheric F_2 density peak, where the refractive index abruptly decreases owing to the sudden plasma density decrease. DEMETER then detects these reflected waves at lower geomagnetic latitudes. To show the possibility of such propagation, we employed a ray-tracing simulation using a 3-D ray-tracing code with continuous verification of the Wentzel-Kramers-Brillouin (WKB) approximation of geometric optics, described by *Santolík et al.* [2009]. Our objective is to initiate the ray-tracing procedure with the observed wave vectors of earthward propagating waves at the spacecraft position and then compare the theoretical θ_{kB} values of the ionospherically reflected waves with the observed values in the appropriate latitudinal range. Since the values

of ϕ_{kB} are always close to ±180°, we restricted our study to the meridional plane where the ray was described by Cartesian coordinates x, z linked to the Earth's magnetic field dipole axis.

The ray-tracing simulation was done under the cold plasma approximation with a dipole model of the Earth's magnetic field and with the diffusive equilibrium (DE) model of the plasma density distribution. We simulated the propagation of QP emissions below the altitude of DEMETER in two steps: The first step was a simulation of the wave propagation from the altitude of DEMETER downward to the ionosphere. The simulation was stopped at the point where the wave could not propagate any further due to a steep density gradient, i. e., where the limit of the WKB approximation was encountered. At that point we assumed a specular reflection of the wave vector from a plane parallel to Earth's surface. In the second step, the simulation continued from the point of reflection to the altitudes of DEMETER.

To describe the plasma density distribution in the ionospheric region, we used the data from the International Reference Ionosphere (IRI) model [*Bilitza*, 2001], specifically the electron temperature T_e, electron density n_e, ratios of ions O^+, He^+, H^+, and the position of the F_2 peak; all these values were calculated from IRI for a reference level of 660 km. At this level, initial conditions for the DE model used in all runs of our program were $T_e = 2\,200$ K, $n = 13\,800\,\mathrm{cm}^{-3}$, $n(O^+)/n_e = 0.599$, $n(He^+)/n_e = 0.047$, and $n(H^+)/n_e = 0.307$. The height of the base of the F_2 peak was 140 km.

The ray-tracing simulation was conducted for a fixed frequency of 1000 Hz and for different values of the initial λ_{mag} along the spacecraft orbit. In all cases the ionospheric reflection occurs at the altitude of ~160 km, and the rays continue to propagate in the anti-earthward direction, crossing the altitudes of DEMETER at different latitudes depending on their initial wave vector direction. These corresponding initial values of θ_{kB} and λ_{mag} to start ray tracing were taken directly from the measurement—for the purpose of our simulation we used the spectrogram in Figure 1 averaged over eight neighboring time intervals. Examples of resulting rays are plotted in Figure 2a for two particular values of the initial λ_{mag}. Figure 2b shows the initial measured downward θ_{kB} (green) and a comparison of the measured θ_{kB} of upgoing waves (red) with the resulting simulated θ_{kB} of reflected waves (black) at the spacecraft altitude, as a function of λ_{mag}.

At higher latitudes DEMETER observes only the direct waves with θ_{kB} in the interval from 30° to 70°. When it moves by about 2° of λ_{mag} in the direction to equator, it starts detecting the reflected waves, as we can see in the mixed spectra near and below $\lambda_{mag} = 56°$ in Figure 1. In the region of $\lambda_{mag} = 51°–54°$ the reflected waves are prominent, yet a certain amount of direct waves is still present and so the averaged value of θ_{kB} is somewhat smaller than what our simulations show. Because of this effect we left a small gap in λ_{mag} to ensure that the initial values will not contain data obtained by averaging nearly equal numbers of direct and reflected waves. Besides this effect, we can see that the simulated θ_{kB} values of reflected waves are remarkably similar to the observed values.

4. Backward Ray Tracing

With the same ray-tracing procedure and under the same conditions as mentioned above we conducted a backward ray tracing from the altitudes of DEMETER in order to indicate the position of the source region of the studied QP emissions. The appropriate trajectories can be found with forward propagation by reversing the wave vector, since the wave vector inversion is equivalent to the wave propagation back in time.

In these simulations we cannot neglect the existence of the plasmapause. As a measure of geomagnetic activity, which strongly influences the location of the plasmapause [*O'Brien and Moldwin*, 2003], we use the *Kp* index obtained from World Data Center for Geomagnetism, Kyoto. During our measurements the value of the 3 h *Kp* was 2−, while the last 36 h maximum was 4. The profile of the plasmapause has been modeled using a sine function with a relative decrease of density of 0.05 and with a half width of 0.5 R_E. The resulting profiles obtained by modeling the plasmapause with a sine function are nearly indistinguishable (within 3ς*percnt*;) from those that can be obtained with a hyperbolic tangent, which is used, e.g., in the GCPM model described in *Gallagher et al.* [2000]. Based on the value of $Kp = 4$ we have obtained the central position of the plasmapause at $L_{pp} = 4.2 \pm 0.8$, according to the model of *O'Brien and Moldwin* [2003]. We tried to account for the uncertainty of the modeled plasmapause position, but for $L_{pp} < 4.2$ the propagation was stopped very early for almost all initial values due to the violation of the WKB condition. We have therefore used four different values of L_{pp}, 4.2, 4.6, 5.0, and 5.4.

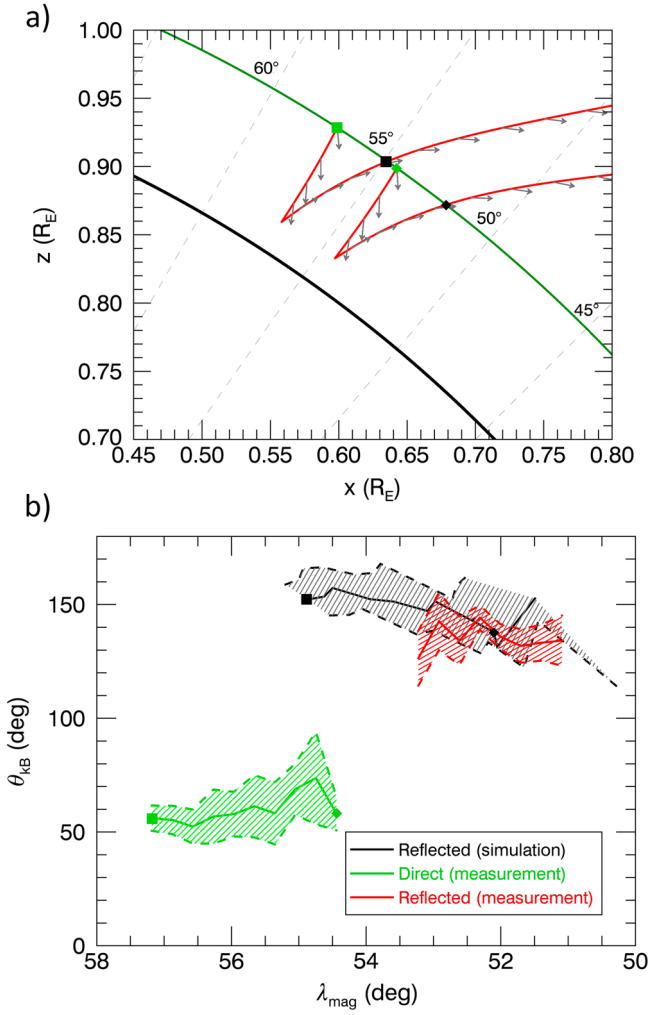

Figure 2. (a) Detail of ionospheric reflection of simulated ray trajectories of whistler mode QP emissions. The thick black curve is the Earth's surface, and the green curve stands for the orbital altitude of the DEMETER satellite. The grey arrows represent the wave vector directions along the path with equidistant group time intervals of 0.01 s. The initial value of λ_{mag} of depicted rays was 54.4° and 57.2°. (b) Dependence of polar angle θ_{kB} on geomagnetic latitude λ_{mag} for observed waves, together with simulated rays crossing the position of DEMETER. Green line connects the initial measured values of θ_{kB} of direct waves, red line connects the final measured values of θ_{kB} for reflected waves. Dashed green and red lines and filled areas represent the standard deviation σ. Black line shows the result of simulation of reflected rays, where the dashed black lines are results of simulation for averaged initial θ_{kB} increased or decreased by σ. The square and diamond symbols refer to Figure 2a, representing direct (green) and reflected (black) rays. The ~ 15 s gap between red and green areas represents the time interval where mixing of direct and reflected waves is most prominent and therefore cannot be used for comparison.

Figure 3 shows the simulated rays along with their wave vectors. We can see that the rays are not ducted by the plasmapause, but they are rather guided by the reflections on the density gradient of its inner boundary. The QP emissions would therefore probably originate close to this boundary. This hypothesis of unducted propagation is consistent with the wave analysis done by *Němec et al.* [2013] on 10 years of Cluster spacecraft data.

In each simulation where the WKB condition was not violated, the ray encountered the lower hybrid frequency before reaching the plasmapause. Building on the assumption that the observed whistlers originate close to the inner boundary of the plasmapause, we infer that the waves are likely generated at frequencies above the local lower hybrid frequency. However, with the obtained low wave normal angles these waves do not reflect when their frequency becomes close to the lower hybrid frequency during their propagation to lower altitudes.

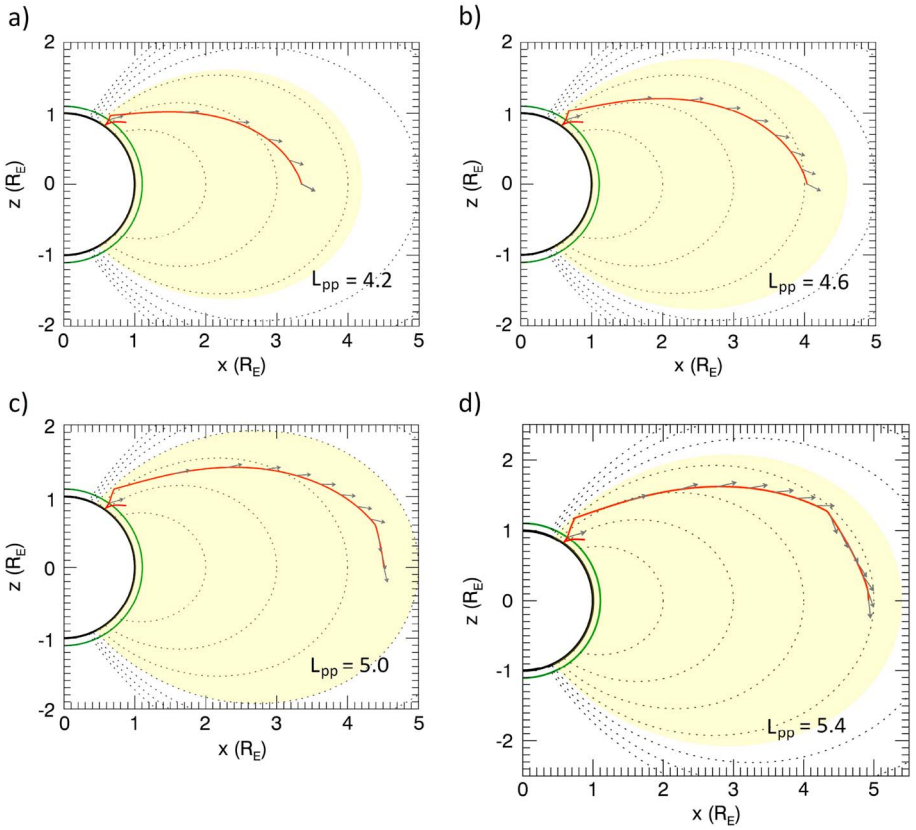

Figure 3. Backward ray tracing for four different plasmapause positions, $L_{pp} = \{4.2, 4.6, 5.0, 5.4\}$. The grey arrows represent the wave vector direction along the raypath with equidistant group time intervals of 0.5 s. The dotted lines are magnetic field lines $L = 2, 3, \ldots$. Yellow area relates to the plasmasphere with the central distance of plasmapause as the boundary. The initial value of λ_{mag} was 55.0° in all four cases.

5. Discussion

Our ray-tracing simulation results show that outgoing waves observed at lower latitudes can be explained by their reflection below the spacecraft orbit. This mechanism has been also proposed by *Santolík and Parrot* [1999] based on observations of the Freja spacecraft, but this hypothesis has not been confirmed yet, as the ray-tracing simulation has not been done for their cases. Extensive studies presented in *Sonwalkar et al.* [2011a] and *Sonwalkar et al.* [2011b] show the specular reflection as one of three mechanisms that can be utilized in remote sensing of the Earth's plasma structure with sounder generated whistler mode echoes. However, the frequency of waves analyzed in *Sonwalkar et al.* [2011b] by means of a ray-tracing simulation was typically above 6 kHz, much higher than in the case presented in this article.

One might also propose a modified propagation scheme where waves penetrate the ionosphere downward, travel for a few hundreds of kilometers in the Earth-ionosphere waveguide, and then leave the guide and penetrate the ionosphere again but in the upward direction [*Fiser et al.*, 2010]. Such a scheme would be possible if the wave vectors of studied electromagnetic waves were perpendicular to the Earth's surface, which is not the case. Additionally, the waves leaving the Earth-ionosphere waveguide would be more attenuated than the waves which were reflected only once, and their wave vectors would also be vertical, which again contradicts the measurements.

Validity of the density model used in our simulation should be scrutinized. Results of the test runs of our simulation with different density models (not shown) indicate that higher reference values of the electron density n_e of the diffusive equilibrium model would only change the group time of waves, while the general shape of their trajectory would be preserved. Height of the ionospheric F_2 peak has a clear impact on the latitudinal difference between the direct and reflected wave. Lower heights would result in a shift of the black area in the $\theta_{kB}(\lambda_{mag})$ plot in Figure 2b to lower latitudes. Opposite trend would be obtained for higher F_2

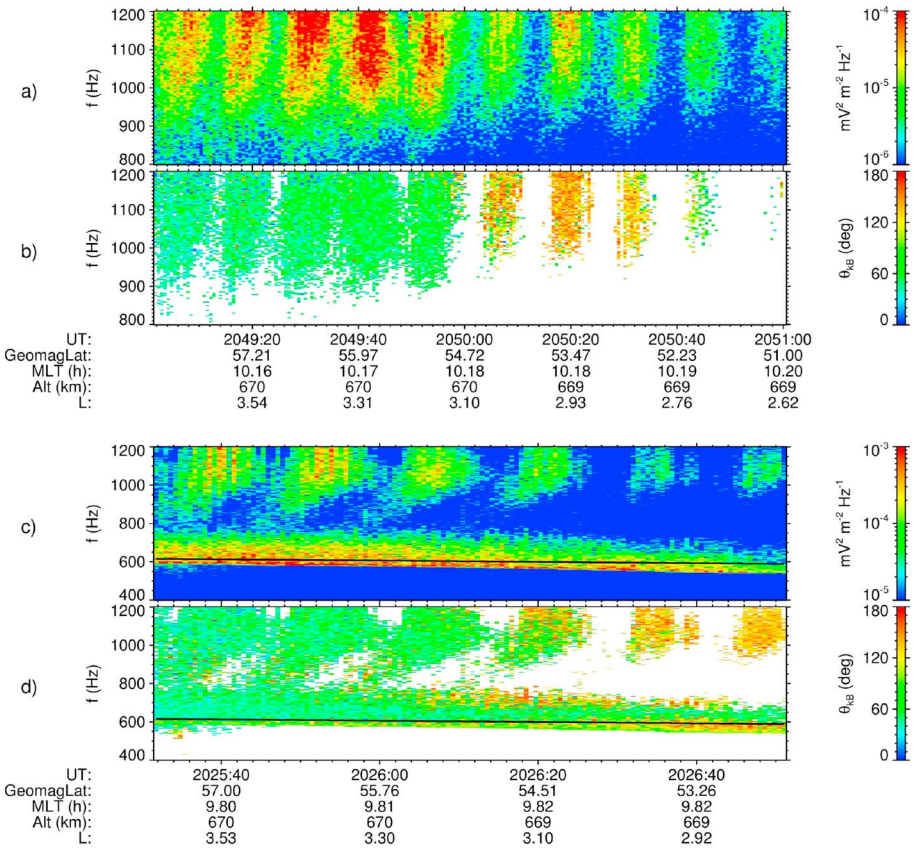

Figure 4. Frequency-time spectrograms of (a, c) electric field power spectral density and (b, d) polar angle θ_{kB} for QP events observed by DEMETER on 9 August 2006 (Figures 4a and 4b) and 1 March 2007 (Figures 4c and 4d). The latter case also shows a strong hiss emission situated around the proton cyclotron frequency (solid line).

heights. In the work of *Sonwalkar et al.* [2011a], it is assumed that the specular reflection occurs at about 90 km, where the ionization is low and the refractive index decreases rapidly. However, our simulation results fit the observations very well if we use the position of the F_2 peak predicted by the IRI model [*Bilitza*, 2001] and assume a specular reflection at the altitude where the violation of WKB condition occurs. At the point of reflection, the value of refractive index is typically between 5 and 10, about an order of magnitude lower than at height of the F_2 peak, where it exceeds the value of 50.

At lower altitudes, we must consider the effects of electron-neutral interactions. According to *Schunk and Nagy* [2004], the momentum transfer collision frequency for the elastic electron-N_2 interactions (which are dominant) depends on the electron temperature and on the nitrogen density. Using the electron temperature obtained from the IRI model and the nitrogen density taken from the Mass Spectrometer and Incoherent Scatter model [*Schunk and Nagy*, 2004], we obtain collision frequencies of $\sim 300\,s^{-1}$ and $\sim 60\,s^{-1}$ at altitudes of 160 km and 200 km, respectively. The value $300\,s^{-1}$ is roughly of the same order of magnitude as the frequency $f = 1000$ Hz used in our ray-tracing simulation. Thus, close to the lowest altitudes encountered in the simulation, the electron-neutral collisions are not negligible. However, it should be noted that collisions affect mainly the wave amplitude, not the ray trajectories. Therefore, the effect of collisions was not included in our simulations.

Propagation of QP emissions from their source region depends on whether the whistler mode waves are ducted or unducted [*Santolík et al.*, 2006; *Titova et al.*, 2015]. In our case simulations show that the waves are not ducted but that their source region is clearly dependent of the position of plasmapause, as we can see from the backward traced rays in Figure 3. Plasmapause may in a general case act as a duct [*Woodroffe and Streltsov*, 2013], but from the backward ray tracing we infer that ducted waves would not correspond to the observed θ_{kB} values. However, the presence of the plasmapause is necessary because the waves reflect on the

inner boundary density gradients, and thus, they acquire the Poynting and wave vector directions which are consistent with DEMETER observations.

Ongoing research of QP waves with unique behavior on small latitudinal scales is important since they are naturally smoothed out in large statistics due to averaging [*Hayosh et al.*, 2016]. Figure 4 presents spectrograms of power spectral density of electric field and θ_{kB} angle for another two QP events showing the same characteristics as the event we have analyzed in Figure 1. Event from 9 August 2006, 20:49–20:51 UT (Figures 4a and 4b) as well as the event of 1 March 2007, 20:25–20:27 again shows reflected upgoing waves at lower latitudes, with similar evolution of θ_{kB} as in Figure 1c. The 3 h *Kp* index for the event from 9 August 2006 was 1, and the last 36 h maximum was 3. These respective values of *Kp* indices for the event from 1 March 2007 were 1 and 4+. These levels are very similar to those measured for the event observed on 13 April 2006; therefore, the estimate of the plasmapause central distance also stays similar ($L_{pp} = 4.0 \pm 0.8$ for 9 August 2006 and $L_{pp} = 4.6 \pm 0.8$ for 1 March 2007).

The conclusion of our study is that QP emissions observed by a spacecraft at a low altitude orbit can exhibit a sudden change of the wave and Poynting vector directions in a very narrow interval of geomagnetic latitudes, and that this behavior can be explained by an ionospheric reflection of electromagnetic waves. We have presented simulations based on ray tracing in a cold plasma that strongly support this propagation scheme. We have also shown that the source region of these waves may be located on the inner boundary of the plasmapause, and that the waves are guided by reflections on the plasmapause density gradient.

Acknowledgments
This work is mainly related to data recorded by the microsatellite DEMETER which was operated by the French Centre National d'Etudes Spatiales (CNES). The DEMETER data shown in this paper can be obtained at https://cdpp-archive.cnes.fr/. Work of M. Hanzelka, O. Santolik, and M. Hajoš was supported by MSMT grant LH 15304, GACR grant 17-07027S, and by the Praemium Academiae award from the CAS. Work of F. Nemec was supported by GACR grant 15-01775Y.

References

Bespalov, P. A. (1981), Self-modulation of radiation of a plasma cyclotron "maser", *JETP Let.*, *33*, 182–185.
Bilitza, D. (2001), International reference ionosphere 2000, *Radio Sci.*, *36*, 261–275, doi:10.1029/2000RS002432.
Bortnik, J., L. Chen, W. Li, R. M. Thorne, and R. B. Horne (2011), Modeling the evolution of chorus waves into plasmaspheric hiss, *J. Geophys. Res.*, *116*, A08221, doi:10.1029/2011JA016499.
Davidson, G. T. (1979), Self-modulated VLF wave-electron interactions in the magnetosphere—A cause of auroral pulsations, *J. Geophys. Res.*, *84*, 6517–6523, doi:10.1029/JA084iA11p06517.
Fiser, J., J. Chum, G. Diendorfer, M. Parrot, and O. Santolik (2010), Whistler intensities above thunderstorms, *Ann. Geophys.*, *28*(11), 37–46, doi:10.5194/angeo-28-37-2010.
Gallagher, D. L., P. D. Craven, and R. H. Comfort (2000), Global core plasma model, *J. Geophys. Res.*, *105*, 18,819–18,833, doi:10.1029/1999JA000241.
Hayosh, M., D. L. Pasmanik, A. G. Demekhov, O. Santolik, M. Parrot, and E. E. Titova (2013), Simultaneous observations of quasi-periodic ELF/VLF wave emissions and electron precipitation by DEMETER satellite: A case study, *J. Geophys. Res. Space Physics*, *118*, 4523–4533, doi:10.1002/jgra.50179.
Hayosh, M., F. Němec, O. Santolík, and M. Parrot (2016), Propagation properties of quasiperiodic VLF emissions observed by the DEMETER spacecraft, *Geophys. Res. Let.*, *43*, 1007–1014, doi:10.1002/2015GL067373.
Helliwell, R. A. (1965), *Whistlers and Related Ionospheric Phenomena*, Stanford Univ. Press, Stanford, Calif.
Kimura, I. (1974), Interrelation between VLF and ULF emissions, *Space Sci. Rev.*, *16*, 389–411, doi:10.1007/BF00171565.
Němec, F., O. Santolík, J. S. Pickett, M. Parrot, and N. Cornilleau-Wehrlin (2013), Quasiperiodic emissions observed by the Cluster spacecraft and their association with ULF magnetic pulsations, *J. Geophys. Res. Space Physics*, *118*, 4210–4220, doi:10.1002/jgra.50406.
O'Brien, T. P., and M. B. Moldwin (2003), Empirical plasmapause models from magnetic indices, *Geophys. Res. Lett.*, *30*, 1152, doi:10.1029/2002GL016007.
Pasmanik, D., A. Demekhov, V. Trakhtengerts, and M. Parrot (2004), Modeling whistler wave generation regimes in magnetospheric cyclotron maser, *Ann. Geophys.*, *22*, 3561–3570, doi:10.5194/angeo-22-3561-2004.
Santolík, O., and D. A. Gurnett (2002), Propagation of auroral hiss at high altitudes, *Geophys. Res. Lett.*, *29*, 1481, doi:10.1029/2001GL013666.
Santolík, O., and M. Parrot (1999), Case studies on the wave propagation and polarization of ELF emissions observed by Freja around the local proton gyrofrequency, *J. Geophys. Res.*, *104*, 2459–2476, doi:10.1029/1998JA900045.
Santolík, O., M. Parrot, and F. Lefeuvre (2003), Singular value decomposition methods for wave propagation analysis, *Radio Sci.*, *38*, 1010, doi:10.1029/2000RS002523.
Santolík, O., F. Němec, M. Parrot, D. Lagoutte, L. Madrias, and J. J. Berthelier (2006), Analysis methods for multi-component wave measurements on board the DEMETER spacecraft, *Planet. Space Sci.*, *54*, 512–527, doi:10.1016/j.pss.2005.10.020.
Santolík, O., M. Parrot, U. S. Inan, D. Burešová, D. A. Gurnett, and J. Chum (2009), Propagation of unducted whistlers from their source lightning: A case study, *J. Geophys. Res.*, *114*, A03212, doi:10.1029/2008JA013776.
Santolík, O., J. S. Pickett, D. A. Gurnett, J. D. Menietti, B. T. Tsurutani, and O. Verkhoglyadova (2010), Survey of Poynting flux of whistler mode chorus in the outer zone, *J. Geophys. Res.*, *115*, A00F13, doi:10.1029/2009JA014925.
Sato, N., K. Hayashi, S. Kokubun, T. Oguti, and H. Fukunishi (1974), Relationships between quasi-periodic VLF emission and geomagnetic pulsation, *J. Atmos. Terr. Phys.*, *36*, 1515–1526.
Sazhin, S. S., and M. Hayakawa (1994), Periodic and quasiperiodic VLF emissions, *J. Atmos. Terr. Phys.*, *56*, 735–753.
Schunk, R. W., and A. F. Nagy (2004), *Ionospheres*, 570 pp., Cambridge Univ. Press, Cambridge.
Smith, A. J., M. J. Engebretson, E. M. Klatt, U. S. Inan, R. L. Arnoldy, and H. Fukunishi (1998), Periodic and quasiperiodic ELF/VLF emissions observed by an array of Antarctic stations, *J. Geophys. Res.*, *103*, 23,611–23,622, doi:10.1029/98JA01955.
Sonwalkar, V. S., D. L. Carpenter, A. Reddy, R. Proddaturi, S. Hazra, K. Mayank, and B. W. Reinisch (2011a), Magnetospherically reflected, specularly reflected, and backscattered whistler mode radio-sounder echoes observed on the IMAGE satellite: 1. Observations and interpretation, *J. Geophys. Res.*, *116*, A11210, doi:10.1029/2011JA016759.

Sonwalkar, V. S., A. Reddy, and D. L. Carpenter (2011b), Magnetospherically reflected, specularly reflected, and backscattered whistler mode radio-sounder echoes observed on the IMAGE satellite: 2. Sounding of electron density, ion effective mass (m_{eff}), ion composition (H^+, He^+, O^+), and density irregularities along the geomagnetic field line, *J. Geophys. Res.*, *116*, A11211, doi:10.1029/2011JA016760.

Titova, E. E., B. V. Kozelov, A. G. Demekhov, J. Manninen, O. Santolik, C. A. Kletzing, and G. Reeves (2015), Identification of the source of quasiperiodic VLF emissions using ground-based and Van Allen Probes satellite observations, *Geophys. Res. Lett.*, *42*, 6137–6145, doi:10.1002/2015GL064911.

Tixier, M., and N. Cornilleau-Wehrlin (1986), How are the VLF quasi-periodic emissions controlled by harmonics of field line oscillations?—The results of a comparison between ground and GEOS satellites measurements, *J. Geophys. Res.*, *91*, 6899–6919, doi:10.1029/JA091iA06p06899.

Woodroffe, J. R., and A. V. Streltsov (2013), Whistler propagation in the plasmapause, *J. Geophys. Res. Space Physics*, *118*, 716–723, doi:10.1002/jgra.50135.